J. Fluid Mech. (1978), *vol.* 85, *part* 2, *pp.* 273–303
Printed in Great Britain

The structure of turbulent boundary layers along mildly curved surfaces

By B. R. RAMAPRIAN
Institute of Hydraulic Research, University of Iowa, Iowa City
AND B. G. SHIVAPRASAD
Aeronautical Engineering Department, Indian Institute of Science, Bangalore

(Received 27 September 1976 and in revised form 18 July 1977)

This paper describes a detailed study of the structure of turbulence in boundary layers along mildly curved convex and concave surfaces. The surface curvature studied corresponds to $\delta/R_w = \pm 0{\cdot}01$, δ being the boundary-layer thickness and R_w the radius of curvature of the wall, taken as positive for convex and negative for concave curvature. Measurements of turbulent energy balance, autocorrelations, auto- and cross-power spectra, amplitude probability distributions and conditional correlations are reported. It is observed that even mild curvature has very strong effects on the various aspects of the turbulent structure. For example, convex curvature suppresses the diffusion of turbulent energy away from the wall, reduces drastically the integral time scales and shifts the spectral distributions of turbulent energy and Reynolds shear stress towards high wavenumbers. Exactly opposite effects, though generally of a smaller magnitude, are produced by concave wall curvature. It is also found that curvature of either sign affects the v fluctuations more strongly than the u fluctuations and that curvature effects are more significant in the outer region of the boundary layer than in the region close to the wall. The data on the conditional correlations are used to study, in detail, the mechanism of turbulent transport in curved boundary layers.

1. Introduction

Several studies in the past (e.g. Wattendorf 1935; Schmidbauer 1936; Patel 1968) have shown that the behaviour of the turbulent boundary layer is very sensitive to longitudinal wall curvature. Bradshaw (1969) showed that even a very mild longitudinal curvature (say $\delta/R_w \approx \frac{1}{300}$, δ being the boundary-layer thickness and R_w the wall radius, taken positive for convex wall curvature and negative for concave curvature) can significantly affect the length-scale distribution in the boundary layer and hence the flow development. Subsequent work by others confirmed this. It is now fairly well known that convex wall curvature inhibits turbulence while concave curvature enhances it. It is also known (Eskinazi & Yeh 1956) that the wall shear stress is larger on the concave wall than on the convex wall of a curved duct. The explanation given for these effects stems from stability arguments. A lump of turbulent fluid is in a state of stable equilibrium over a convex wall whereas it will be in a state of unstable equilibrium over a concave wall. Hence momentary disturbances

(turbulent motions) are damped in one case (convex wall) and amplified in the other (concave wall). There thus seems to be a strong analogy between the effects of curvature and buoyancy. In fact, on the basis of such an analogy, Bradshaw (1969) estimated the effect of streamline curvature on the mixing length l_m in a boundary layer by using the following equations:

$$\left.\begin{aligned} l_{mf}/l_m &= 1+\beta R_{ic} \quad \text{for convex curvature, i.e.} \quad R_{ic} > 0, \\ l_m/l_{mf} &= 1-2R_{ic} \quad \text{for concave curvature, i.e.} \quad R_{ic} < 0 \\ &\qquad\qquad (\text{valid only for} \quad -0{\cdot}5 < R_{ic} < 0), \end{aligned}\right\} \tag{1.1}$$

where l_{mf} is the mixing length in a flat-wall boundary layer. The term R_{ic} was called by Bradshaw the 'curvature Richardson number' and was defined as

$$R_{ic} = \left\{2(\overline{U}/R)^2 \frac{\partial}{\partial y}(\overline{U}R)\right\} \Big/ (\partial \overline{U}/\partial y)^2,$$

where R is the radius of curvature of the streamline. Subsequent workers incorporated Bradshaw's recommendation (1.1) in calculation procedures for boundary layers over curved surfaces. While there are not sufficient experimental data available in this area, in the few cases where the data are available predictions from these calculations agree reasonably well with measurements (e.g. Rastogi & Whitelaw 1971; Papailiou, Nurzia & Satta 1972; Johnston & Eide 1976; Meroney & Bradshaw 1975).

While it has been known for quite some time that streamline curvature affects the structure of turbulence, much of the *detailed* study reported in this area is very recent. This fact is brought out by reference to a review article by Bradshaw (1973). Since then, a few detailed investigations have been reported. These are the studies of So & Mellor (1972, 1973, 1975), Ellis & Joubert (1974), So (1975), Meroney & Bradshaw (1975), Irwin & Smith (1975) and Castro & Bradshaw (1976). The experiments of So & Mellor (1972) provided the first detailed turbulence measurements in curved boundary layers. They measured turbulent intensities and shear stress in boundary layers over both convex and concave walls. Castro & Bradshaw (1976) studied the effect of streamline curvature in highly sheared mixing layers. Their measurements included, in addition to turbulent intensities and Reynolds shear stress, a detailed turbulent energy balance.

The experimental studies mentioned above relate to strong streamline curvature ($|\delta/R_w| \approx 0{\cdot}1$ in the experiments of So & Mellor and $\delta/R \approx 0{\cdot}2$ in the experiments of Castro & Bradshaw). Unfortunately, there is virtually no detailed work of a similar kind reported for mild curvature, with the single exception of the recent study by Meroney & Bradshaw (1975). They made measurements of turbulent intensities and Reynolds shear stress in curved boundary layers with $\delta/R_w \approx \pm 0{\cdot}01$. This value of δ/R_w is in the same range as that studied by the present authors.

When the present investigation was started, there were very few data on curvature effects in turbulent boundary layers. The authors undertook a comprehensive study of the effect of mild wall curvature ($\delta/R_w \approx \pm 0{\cdot}013$) on the behaviour of the turbulent boundary layer. The investigation included an experimental study of both the mean and the turbulent structure of the flow and is fully described in Shivaprasad (1976). While the investigation was in progress, several other reports mentioned earlier appeared. However, the authors believe that the present study has gone further than the other investigations reported so far, especially with regard to *mild* curvature

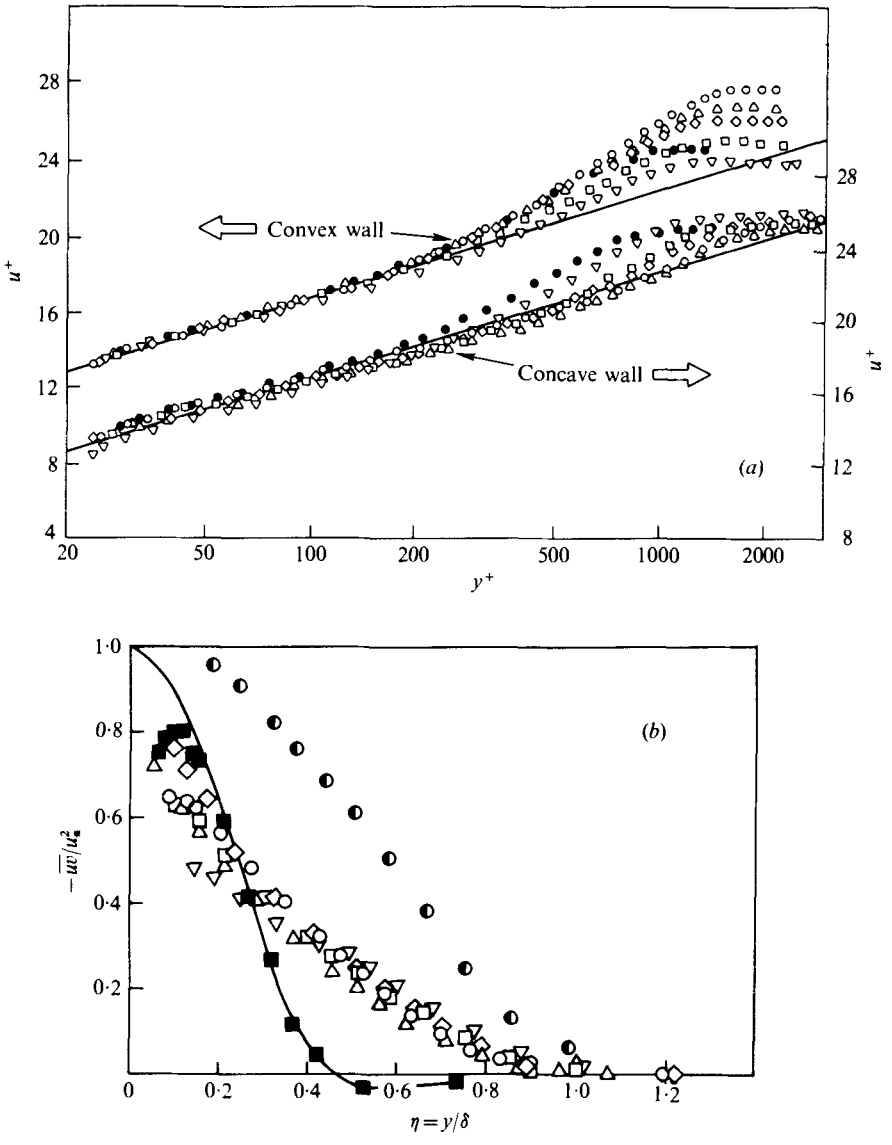

FIGURES 1 (*a*, *b*). For legend see next page.

effects. The mean flow study brought out some significant points not hitherto adequately reported in the literature and is reported separately (Ramaprian & Shivaprasad 1977). The measurements of turbulence intensities and shear stress were used to study the applicability of some of the phenomenological models of turbulence in the presence of streamline curvature. The shear-stress data were also used to examine the effect of curvature on the mixing length, thus providing the first *direct* test of Bradshaw's recommendations represented by (1.1). This part of the study is also reported elsewhere (Shivaprasad & Ramaprian 1977).

The study of the distributions of the mean and turbulent quantities across the boundary layer revealed that even mild curvature has a very strong effect on the

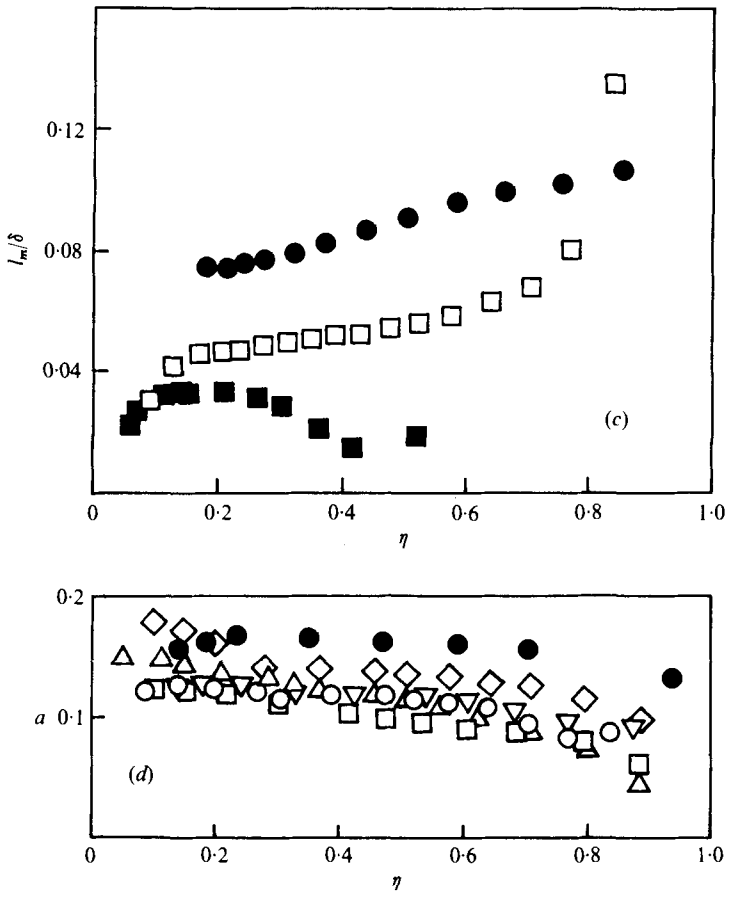

FIGURE 1. Some typical results for curved-wall boundary layers from Shivaprasad & Ramaprian (1977). (*a*) Mean velocity distributions across the curved boundary layers. Station: ●, 20; ▽, 23; □, 26; ◇, 29; △, 32; ○, 35. ——, $u^+ = 5{\cdot}6 \log y^+ + 5{\cdot}5$. (Station designations are explained in figure 2.) (*b*) Reynolds shear stress distribution across the convex-wall boundary layer. Station: ◐, 20; ▽, 23; □, 26; ◇, 29; △, 32; ○, 35. —■—, data of So & Mellor (1972) corresponding to a station 23 in. downstream of the beginning of curvature. (*c*) The distribution of the Prandtl mixing length across the boundary layer. ●, flat wall (station 20); □, convex wall (station 35); ■, convex-wall experiments of So & Mellor (1972) 23 in. downstream from beginning of curvature. (*d*) The distribution of the structure parameter a across the boundary layer. Symbols as in (*a*).

behaviour of the boundary layer. This can be seen typically from figures 1 (*a*)–(*d*), which are taken from Ramaprian & Shivaprasad (1977) and Shivaprasad & Ramaprian (1977). The designation of the measuring stations is explained in figure 2. In fact, the measurements indicated that the effect of mild curvature is stronger than what one might expect from a linear interpolation between zero and strong curvature. This becomes apparent from a reference to figures 1 (*b*)–(*d*). In figures 1 (*b*) and (*c*) the data for mild convex curvature on the distributions of the Reynolds shear stress $-\rho\overline{uv}$ and the mixing length l_m are compared with the (available) data for strong convex curvature of So & Mellor (1972). The 'disproportionately large' effect of mild curvature is apparent when one remembers that the curvature in the latter case is about 10 times stronger than that in the former. The same conclusion is again reached when

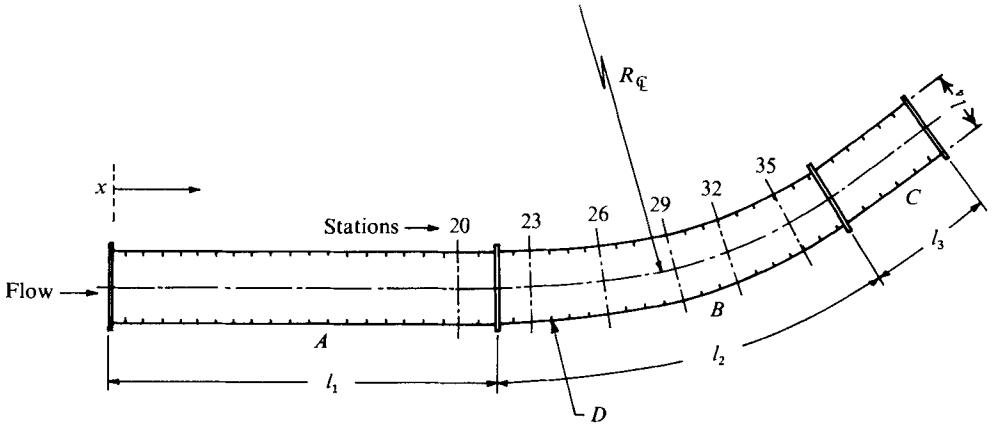

FIGURE 2. Details of the test section. $l_1 = 4$ ft, $l_2 = 3$ ft 11 in., $l_3 = 1$ ft, $l_4 = 4$ in. *A*, inlet straight section; *B*, curved section (10×4 in.); *C*, exit straight section; *D*, wall static taps. The radius of curvature $R_{\mathbb{C}}$ of the centre-line of the test section is 100 in.

Station ...		20	23	26	29	32	35
x (in.)	Convex wall	40·6	50·5	59·3	68·2	77·0	85·8
	Concave wall	40·6	50·8	59·9	69·1	78·3	87·5

the values of the structure parameter $a = -\overline{uv}/\overline{q^2}$ (ranging from 0·12 to 0·07 across the boundary layer and shown in figure 1*d*) are compared with the value of about 0·07 observed by Castro & Bradshaw in a curved mixing layer with $\delta/R \approx 0{\cdot}2$. Figures 1(*a*)–(*d*) will be referred to again later in this report but are introduced here to serve as a background for the detailed study reported in the present paper. The 'large' effect of mild curvature on the turbulent boundary layer provided the motivation for studying these flows in even greater detail. The combination of large effects and very small streamline curvature allows measurements to be made easily and accurately using conventional hot-wire techniques. Yet, because of the nonlinear nature of the curvature effect mentioned above, results obtained for mild curvature are likely to be qualitatively valid for stronger curvatures also. In any case, the mild curvature results are useful in their own right, since mildly curved boundary layers are often encountered in practice (e.g. in aircraft and turbomachinery applications). The results reported in the present paper include measurements of turbulent energy balance, autocorrelations, energy spectra, amplitude probability distributions and conditional correlations of turbulent fluctuations. At the end, the structure of turbulent transport within the boundary layer is discussed in the light of the data obtained.

2. The experimental programme

2.1. *The apparatus*

The test section in which the experiments were carried out is shown schematically in figure 2. A more detailed description of the test facility is given in Shivaprasad (1976). The 10 in. high side walls of the 10×4 in. test section were used as the working surfaces. The initial 4 ft long straight section ensured that a fully developed turbulent boundary layer had formed before the flow reached the curved walls. This was checked

by comparing the distributions of the mean velocity $\bar{v}$, the turbulence velocities u' and v', the turbulent shear stress $-\rho\overline{u'v'}$, the energy spectra of u' and v' and the spectrum of $\overline{u'v'}$ with those for a fully developed flat-plate boundary layer (e.g. Klebanoff 1954; Bradshaw 1967). At the test velocity of 70 ft s^{-1}, the boundary layers developing along the convex and concave side walls did not meet each other even at the end of the curved test section. There was, in fact, a 'free stream' about $\frac{3}{4}$ in. thick at station 35, where the detailed measurements were made. The turbulence intensity in the free stream was about 0·3 %. The radii of the convex and concave walls were 98 in. and 102 in., respectively. The value of $|\delta/R_w|$ varied slightly along the walls. However, a nominal value of 0·013 will be used in this paper to characterize the present wall curvature. The longitudinal pressure gradient was nominally zero but, in fact, a mildly favourable pressure gradient existed along the test section owing to the blockage effect of the boundary layers along the walls. This was, however, checked and it was ensured that this pressure gradient was too small to affect the results presented in this paper in any significant way.

Since it was planned to make very detailed measurements, it became necessary to limit the observations to one typical longitudinal location on each wall, so that the amount of data to be handled could be kept down to a manageable level. Station 35 was selected for the detailed measurements over both walls. This location corresponded to a region where the flow was developing with a sustained curvature effect only, the effect of the sudden change in wall curvature having died down. It can be seen from figures 1 (*a*)–(*d*) that, while the flow has not strictly reached equilibrium on either wall at station 35, there are no large variations in the distributions of the various flow quantities in the streamwise direction around station 35. Another important thing which can be observed is that the various distributions are qualitatively the same at all the locations. Station 35 being the last station, the boundary-layer thicknesses on both the walls were largest at that station. It was therefore easier to make measurements at smaller values of y/δ. Further, since the Reynolds numbers R_θ were reasonably large at this station for both the walls and not too different from each other (approximately 4600 for convex wall and 5000 for concave wall), it would be fairly realistic to make a comparison between the observations on the two walls. The boundary-layer thickness δ (based on 0·995 of the inviscid angular momentum) at this station was 1·16 in. over the convex wall and 1·52 in. over the concave wall. The boundary-layer thickness over the flat wall at station 20 was 0·78 in.

All the measurements were made in a horizontal plane at the midheight of the test section. Checks (see So & Mellor 1972) such as momentum balance, yaw probe traverse for flow inclinations and measurement of the Reynolds shear stress component $-\rho\overline{u'w'}$ were made to assess the magnitude of the secondary flows at station 35. The details of these checks and the results are reported in Shivaprasad (1976). It was found that there were no significant secondary flows within a distance of 1 in. on either side of the plane of measurement.

A significant point to be mentioned here is that, even after many careful tests, it was not possible to detect, in the present experiments, the presence of any organized longitudinal vortices of the Taylor–Görtler type over the concave wall. This is surprising since other investigators have reported their presence both in strongly and mildly curved flows (Tani 1962; So & Mellor 1972, 1975; Meroney & Bradshaw 1975). It is perhaps possible that the rather small aspect ratio, viz. 2·5, of the present test

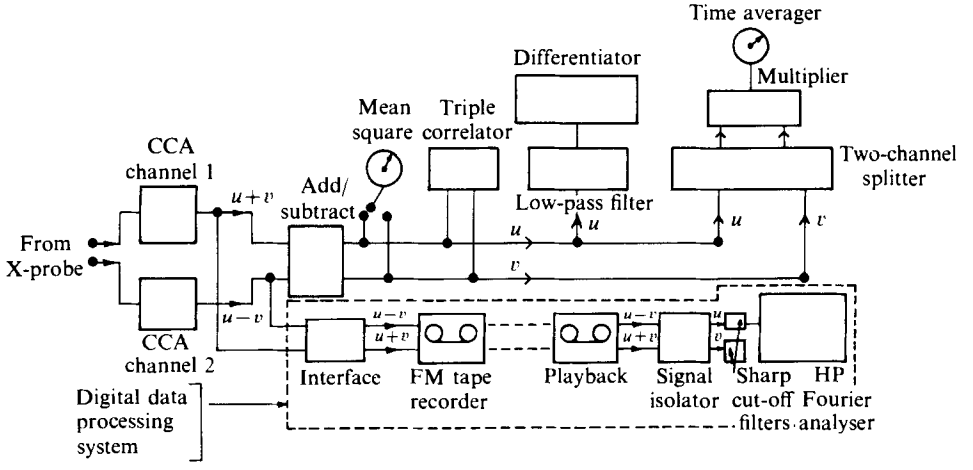

FIGURE 3. Schematic diagram of instrumentation.

section and the consequent strong secondary flows in the *off-centre* planes might have either suppressed these vortices completely or at least rendered them too weak to be detected. Hence the data for the concave wall have been presented only for the midplane and it can be assumed that there was negligible organized spanwise variation observed in the behaviour of the boundary layer.

2.2. *Instrumentation and data processing*

Mean velocity measurements were made using a total-head tube together with a disk-type static pressure tube. Turbulence measurements were made using a dual-channel constant-current hot-wire anemometer system (CCA) described in Shivaprasad (1976). Both single- and X-wire probes were used. Adequate precautions were taken in the calibration and use of the hot-wire equipment. These are also discussed in detail in the above reference. A schematic diagram of the turbulence instrumentation is shown in figure 3. Turbulent energy balance terms were measured directly from the hot-wire signals. The dual-channel hot-wire system provided simultaneous u and v signals. These were used for the measurement of the triple correlations $\overline{u^2v}$ and $\overline{v^3}$ by employing a four-quadrant multiplier and time averager. The triple correlation $\overline{w^2v}$ was not measured. The diffusive flux $\frac{1}{2}\overline{q^2v}$ was obtained from the assumed relation (see Bradshaw 1967)

$$\tfrac{1}{2}\overline{q^2v} = \tfrac{3}{4}\{\overline{u^2v} + \overline{v^3}\}. \tag{2.1}$$

This is equivalent to assuming that the diffusive flux $\overline{w^2v}$ is given by $\frac{1}{2}(\overline{u^2v} + \overline{v^3})$. The pressure diffusion flux $\overline{pv}/\rho$ was also not measured.

The rate of dissipation ϵ of turbulent kinetic energy was measured by using the approximate relations based on Taylor's hypothesis and the assumption of local isotropy (see Hinze 1959, p. 399):

$$\epsilon = 15\frac{\nu}{\overline{U}^2}\overline{\left(\frac{\partial u}{\partial t}\right)^2}, \tag{2.2}$$

where ν is the kinematic viscosity of the fluid. A single-wire probe of diameter 0·0002 in. and sensing length 0·02 in. was used for this purpose. The sensing length was smaller than the expected Taylor microscale even close to the wall. Differentiation of the u

signal was carried out using a differentiating circuit preceded by a sharp cut-off low-pass filter set at 14 kHz.

With regard to the energy balance measurements it is necessary to point out that the experimental approach was to spend relatively more time and effort on those measurements that were expected to contribute significantly to the understanding of curvature effects, and less time on the rest. For example, a relatively simpler method was used to measure the dissipation rate since the near-wall region, where dissipation terms are important (and also where the present measuring technique is the least accurate), is known to be insignificantly affected by mild curvature (Ramaprian & Shivaprasad 1977; Meroney & Bradshaw 1975). Similarly, the triple correlation term $\overline{w^2v}$ was not directly measured but approximately estimated, because its precise measurement would not have added significantly to the information already provided by the measurement of $\overline{u^2v}$ and $\overline{v^3}$. The exception, of course, is the $\overline{pv}/\rho$ term, which is very important but was not measured owing to physical limitations.

The data on autocorrelations, spectra and amplitude probability distributions were obtained by first recording the hot-wire signals on analog tape and later processing them digitally. The fluctuating signals $u+v$ and $u-v$ from the two wires of the X-wire probe (or the signal u only from the single-wire probe) were recorded simultaneously on two channels of analog tape. The instrument used was a GTC (Genesco Technology Corp.) Model 10-286, 14-channel FM tape recorder. Recording was done at a tape speed of 30 in./s. Record lengths varied from 90 s for measurements near the wall to 240 s for measurements near the outer edge of the boundary layer. The system had a flat frequency response from d.c. to 20 kHz. A suitably designed 'isolator' was used to recover the u and v signals simultaneously from the recorded $u+v$ and $u-v$ signals, during play-back. The u and v signals were then passed through a variable frequency, sharp cut-off, low-pass filter (36 dB/octave). The filtered signals were finally fed to a HP 5451A Fourier analyser for analysis. The filtered signals were first digitized in the Fourier analyser and then processed for obtaining autocorrelations etc. The procedure used for digital data processing conformed to the well-established data processing practice described in recent literature (see, for example, MaGrab & Blomquist 1971), and is explained in detail in Shivaprasad (1977). Special precautions were taken to prevent aliasing errors and statistical instability from affecting the results.

In addition to the measurements described above, measurements were also made of several conditional correlations, using the instantaneous u and v signals from the hot-wire amplifiers. These correlations included $\overline{u_+v_+}$, $\overline{u_+v_-}$, $\overline{u_-v_+}$, $\overline{u_-v_-}$, $\overline{u_+^2}$, $\overline{u_-^2}$, $\overline{v_+^2}$ and $\overline{v_-^2}$, where the subscripts represent the sign of the instantaneous fluctuation with respect to the time-mean value. It can be seen that the first four conditional correlations (to be denoted by the general symbol $(\overline{uv})_c$) represent the contribution from the four quadrants to the Reynolds shear stress $-\rho\overline{uv}$, while the last two pairs represent contributions to the Reynolds normal stresses $\rho\overline{u^2}$ and $\rho\overline{v^2}$ respectively. These conditional correlations were obtained by splitting the instantaneous u and v signals into positive and negative halves (using two splitters of the type described by Wallace, Eckelmann & Brodkey 1972) and correlating the appropriate quantities using an analog multiplier and time averager. The instrumentation used for this purpose is also shown schematically in figure 3. For more details reference may be made to Shivaprasad (1976).

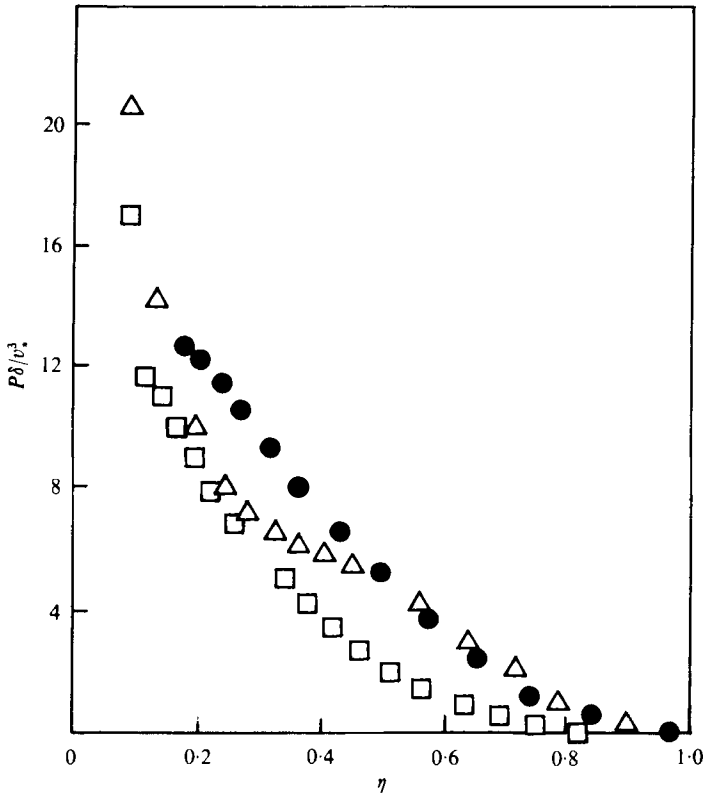

FIGURE 4. The distribution of the rate of turbulent energy production across the boundary layer. □, convex wall; △, concave wall; ●, flat wall. The curved-wall data are for station 35, the flat-wall data for station 20.

3. Results and discussion

3.1. *The turbulent kinetic energy balance*

The turbulent kinetic energy balance was obtained by measuring the terms representing production, dissipation, advection and diffusion in the non-dimensional turbulent kinetic energy equation:

$$\underbrace{\frac{1}{2}\frac{\overline{U}}{u_*}\frac{\partial(\overline{q^2}/u_*^2)}{\partial(x/\delta)}+\frac{1}{2}\frac{\overline{V}}{u_*}\frac{\partial(\overline{q^2}/u_*^2)}{\partial(y/\delta)}}_{\text{advection}}=\underbrace{\frac{\partial}{\partial(y/\delta)}\left\{\frac{\overline{(p/\rho+q^2)v}}{u_*^3}\right\}}_{\text{diffusion}}-\underbrace{\frac{\overline{uv}}{u_*^2}\frac{\partial(\overline{U}/u_*)}{\partial(y/\delta)}}_{\text{production}}-\underbrace{\frac{\epsilon\delta}{u_*^3}}_{\text{dissipation}}, \tag{3.1}$$

where $\overline{V}$ is the mean velocity normal to the wall, p is the turbulent pressure fluctuation and u_* is the friction velocity. Equation (3.1) is strictly applicable only to a flat-wall boundary layer. The exact equation in general orthogonal co-ordinates for two-dimensional flow over a curved surface can be found in So & Mellor (1972). In these co-ordinates, streamline curvature introduces additional terms into the turbulent energy equation. An analysis of the order of magnitude of the various terms in this equation reveals that these additional terms can be neglected if $\delta/R \ll 1$ and if

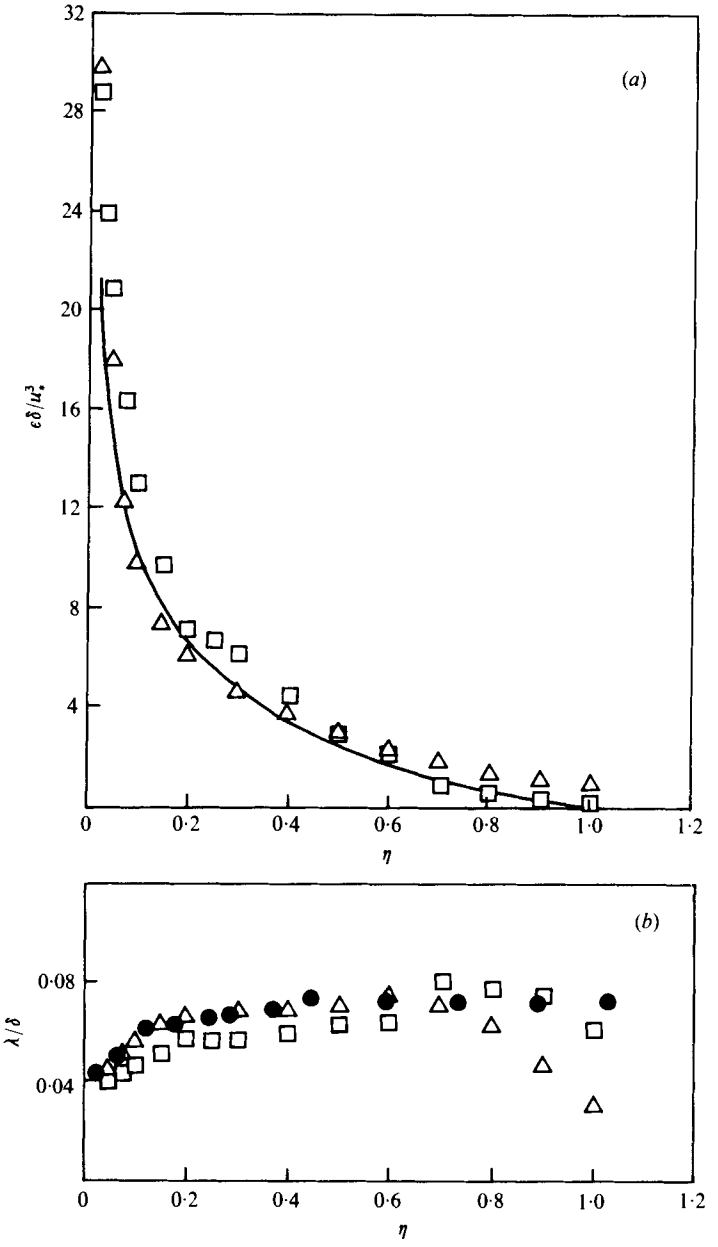

FIGURE 5. The distribution of (*a*) the rate of dissipation and (*b*) the Taylor microscale λ across the boundary layer. □, convex wall (station 35); △, concave wall (station 35); ——, flat wall (from Rajagopalan 1974).

$\phi/R \ll \partial\phi/\partial y$, where $\phi = \overline{U}, \overline{V}, \overline{u^2}, \overline{v^2}, \overline{uv}, \overline{u^2v}$, etc. Since both these conditions were satisfied in the present case, it will be assumed that (3.1) can be used for examining the turbulent energy balance.

The distributions of the rate of production over the two walls are shown in figure 4, along with the distribution for the flat wall at station 20. It is seen that over the convex wall the rate of turbulent energy production falls steeply and is considerably less

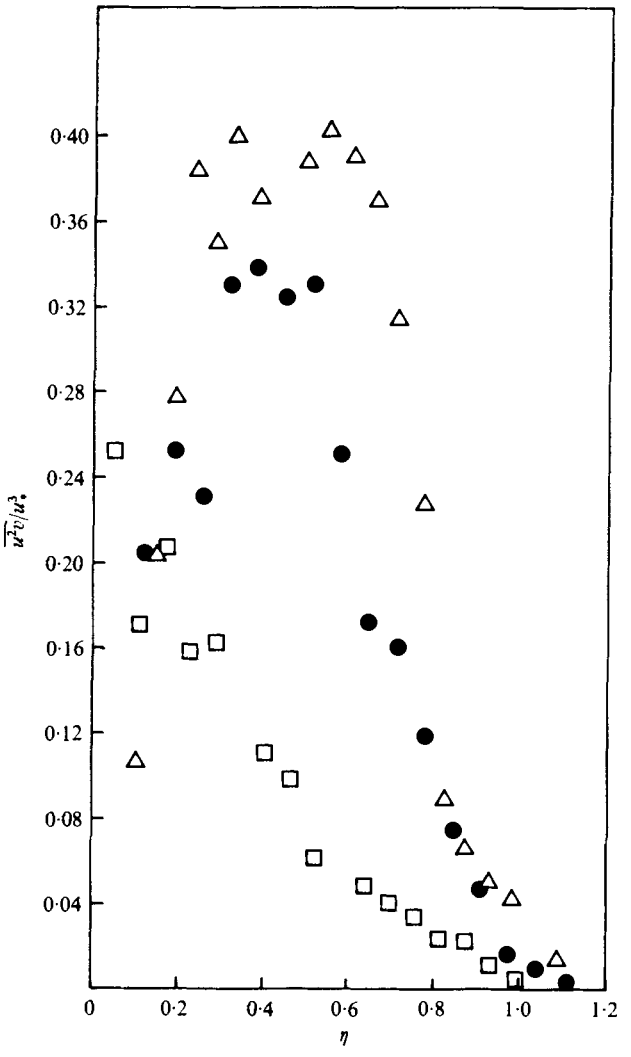

FIGURE 6(*a*). For legend see next page.

than for a flat wall beyond $y/\delta = 0{\cdot}1$. The outer region of the boundary layer over the concave wall, however, does not show any significant deviation from a flat-wall boundary layer with regard to the rate of turbulent energy production.

The distributions of the rate of dissipation for convex, concave and flat walls are shown in figure 5(*a*). The Taylor microscale λ for these three cases, obtained from the formula

$$\lambda^2 = \overline{U}^2 u'^2 \Big/ \overline{\left(\frac{\partial u}{\partial t}\right)^2}, \tag{3.2}$$

is shown in figure 5(*b*). The flat-wall distributions plotted in figures 5(*a*) and (*b*) are from the measurements of Rajagopalan (1974) and correspond roughly to the same Reynolds number as that at station 35. The flat-wall data of the present experiments are not used for comparison. This is because the Reynolds number at station 20 was

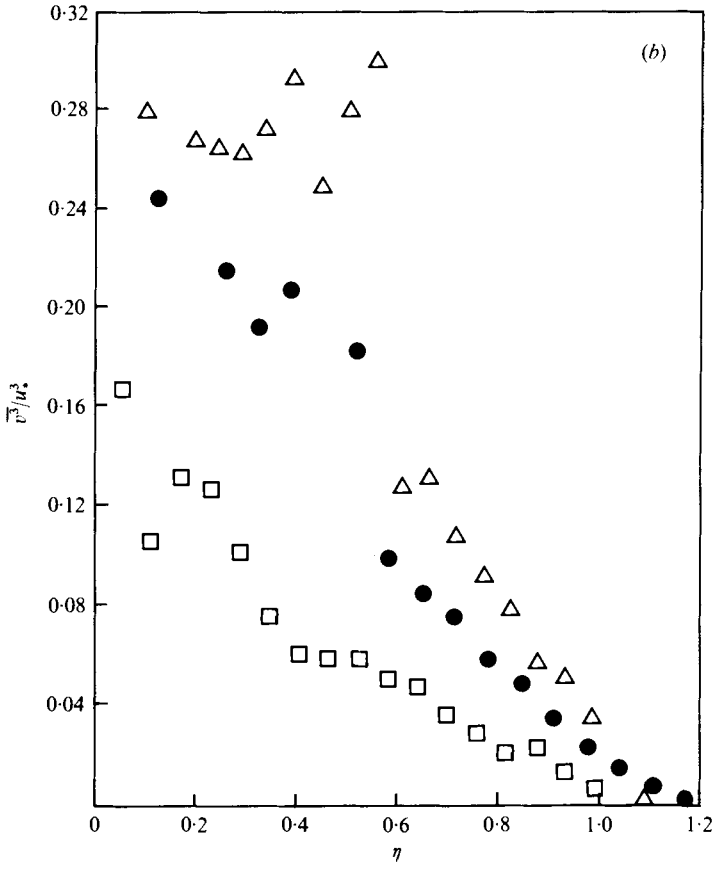

FIGURE 6. The distribution of (*a*) the diffusion flux u^2v/u_*^3 and (*b*) the diffusion flux $\overline{v^3}/u_*^3$ across the boundary layer. Symbols as in figure 4.

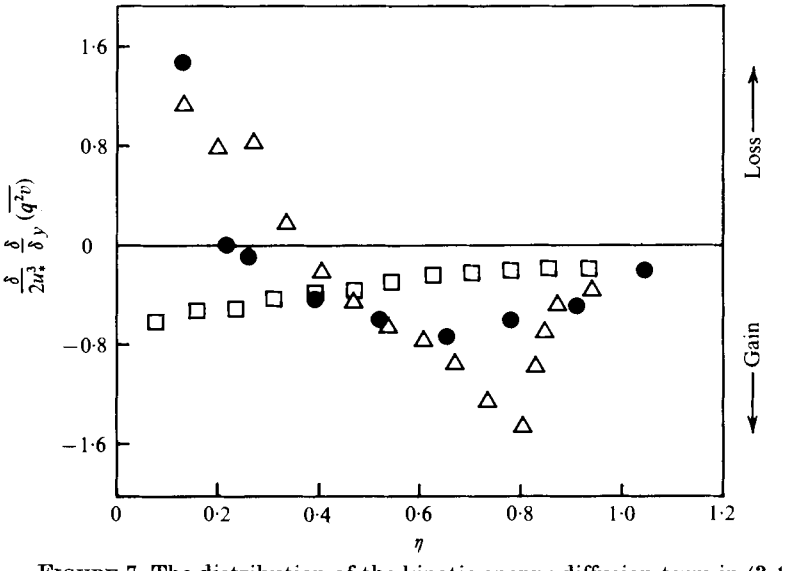

FIGURE 7. The distribution of the kinetic energy diffusion term in (3.1) across the boundary layer. Symbols as in figure 4.

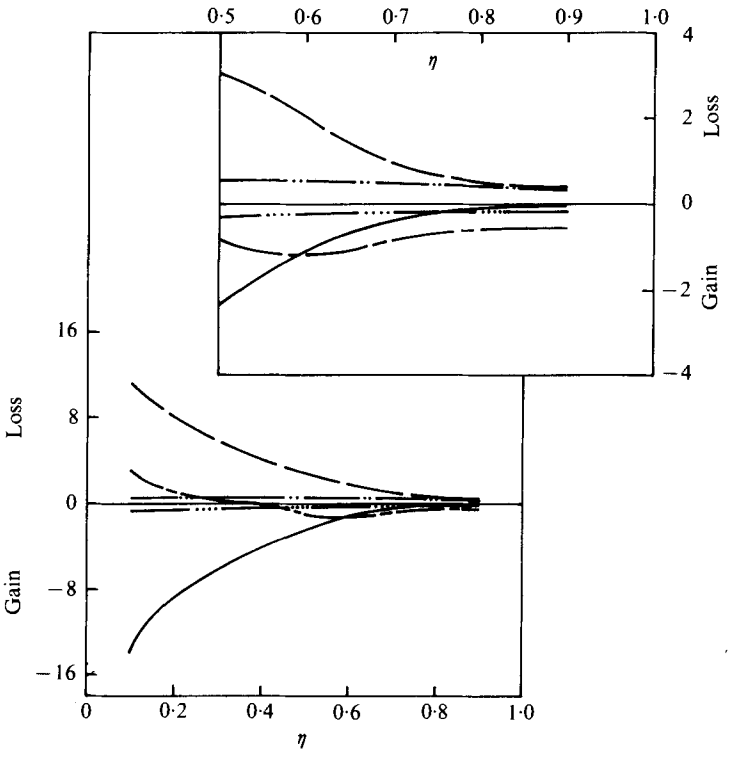

FIGURE 8(*a*). For legend see next page.

small and the dissipation distribution has a strong dependence on Reynolds number, particularly at low Reynolds numbers. It is seen from figure 5(*a*) that (as expected) there is very little difference among the distributions of the dissipation rate over the three walls. A close examination of figure 5(*b*), however, indicates a slightly larger microscale over the concave wall up to a y/δ of about 0·6 compared with the convex wall. The reduction in the microscale for $y/\delta > 0{\cdot}6$ in the case of the concave wall is probably due to the strongly intermittent turbulence structure in the outer layer.

The distributions of the turbulent kinetic energy diffusion fluxes $\overline{u^2v}$ and $\overline{v^3}$ are shown for the three walls in figures 6(*a*) and (*b*). It is seen that the two fluxes exhibit similar trends. The fluxes are larger in the case of the concave wall and very much smaller in the case of the convex wall when compared with the flat wall. The fluxes are everywhere positive, i.e. they are directed away from the wall. As already mentioned, the total turbulent kinetic energy diffusion flux $\frac{1}{2}\overline{q^2v}$ was obtained using (2.1). (The observed similarity in the trends of the $\overline{u^2v}$ and $\overline{v^3}$ distributions suggests that direct measurement of $\overline{w^2v}$ is perhaps not really essential.) The turbulent kinetic energy diffusion term in (3.1) was obtained from this flux distribution by graphical differentiation. The distribution of the diffusion term is plotted for the three walls in figure 7. Figures 8(*a*) and (*b*) show the turbulent kinetic energy balance for the curved-wall boundary layers. In these figures the pressure diffusion term $\overline{pv}/\rho$ is obtained as the closing term in (3.1). Its accuracy should be viewed with some reservation owing to the experimental uncertainties in the measurement of dissipation and diffusion.

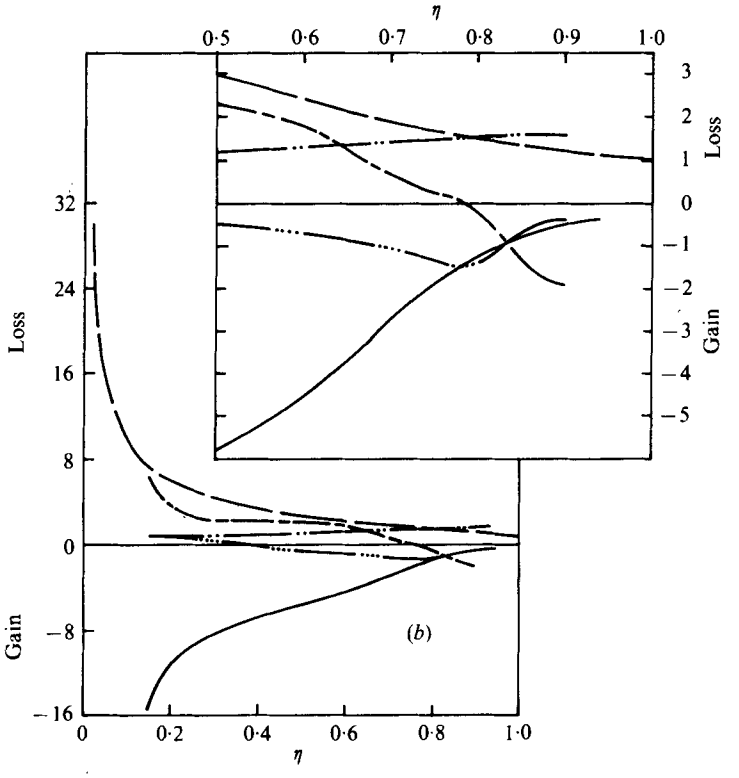

FIGURE 8. Turbulent energy balance for (*a*) the convex-wall and (*b*) the concave-wall boundary layer at station 35. The distributions in the outer layer are shown on an enlarged scale in the figures at the top.

—·—, convection term, $\frac{1}{2}\frac{\delta}{u_*^3}\left[\left(\overline{U}\frac{\overline{\partial q^2}}{\partial x}\right)+\overline{V}\left(\frac{\overline{\partial q^2}}{\partial y}\right)\right]$;

— — —, dissipation term, $\epsilon\delta/u_*^3$;

——, production term, $\frac{\delta}{u_*^3}\left(-\overline{uv}\frac{\partial \overline{U}}{\partial y}\right)$;

—·····—, diffusion term (of turbulent kinetic energy), $\frac{1}{2}\frac{\delta}{u_*^3}\frac{\partial}{\partial y}\overline{(q^2v)}$;

— - —, diffusion term (of pressure), $\frac{\delta}{u_*^3}\frac{\partial}{\partial y}\overline{(p/\rho v)}$ is obtained as the closing term.

Several important features are brought out in figure 7. In the case of the concave wall, the region where there is a net loss of energy by turbulent kinetic energy diffusion extends to a much larger distance from the wall when compared with that for the flat wall. Also, the amount of energy which this region loses to the outer layer is greater. Thus the transport of energy by the turbulent fluctuations is increased and also such transport takes place over a larger distance. Figure 8(*b*) shows that the pressure fluctuations further tend to increase the extent of the region which loses energy to the outer layers and also the magnitude of the diffusion itself. Owing to the increased mixing, a larger region of the outer layer of the concave-wall boundary layer feels the effect of the wall. This is the reason why the log law extends over a larger region and also why the wake-like outer layer is less prominent as can be seen from figure 1(*a*). Exactly the opposite of this happens in the case of the convex wall. The region which

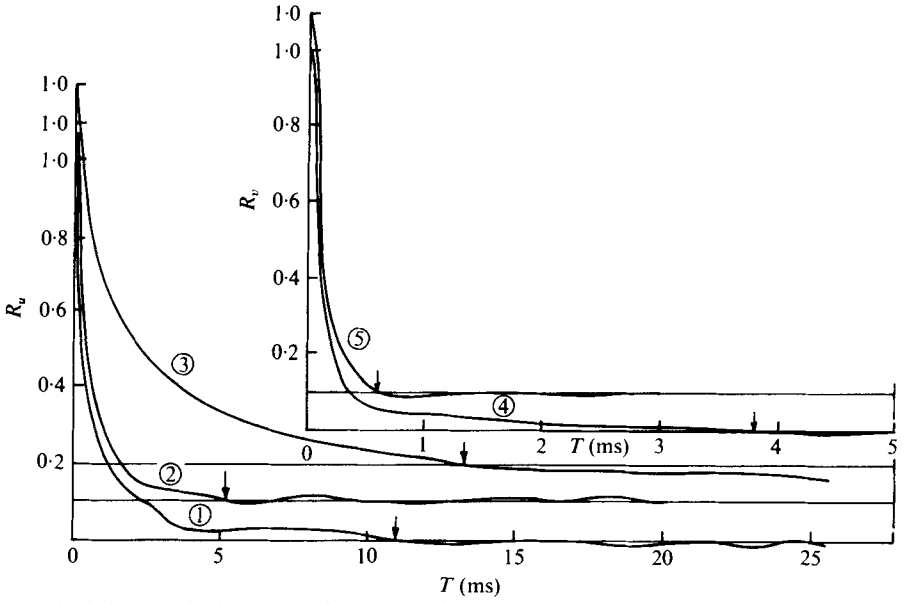

FIGURE 9. A few typical measured autocorrelation curves.

Curve	Component	η	Wall	Station
1	u	0·23	Flat	20
2	u	0·3	Convex	25
3	u	0·3	Concave	35
4	v	0·23	Flat	20
5	v	0·3	Convex	35

Note the change in scale for curves 4 and 5. The arrows indicate the ' last point ' on the correlation curves for computing the area under the curves.

supplies energy to the outer layer is very small and appears to be confined to a very small distance from the wall (perhaps $< 0{\cdot}1\delta$). Unfortunately, no diffusion measurements could be made at points with $y/\delta < 0{\cdot}075$ in the thin boundary layer over the convex wall. However since the diffusion term must integrate to zero across the boundary layer, the required loss due to diffusion must occur very close to the wall. The trend of the data from concave- and flat-wall boundary layers suggests that this is possible. It is clearly seen that, over the convex wall, the transport of turbulent kinetic energy due to the turbulent fluctuations is suppressed. In this case, even the transport due to pressure fluctuations is not very significant as can be seen from figure 8(*a*). This reduced diffusion of turbulent energy results in confining the effect of the wall to a small region near the wall.

3.2. *Autocorrelations*

Correlograms. The autocorrelation coefficients of the fluctuating velocity components u and v at any location (x, y) are defined as

$$R_u(x, y, T) = \overline{u(x, y, t)\, u(x, y, t+T)}/\overline{u^2}(x, y)$$

and

$$R_v(x, y, T) = \overline{v(x, y, t)\, v(x, y, t+T)}/\overline{v^2}(x, y),$$

where T is the time interval between the instants.

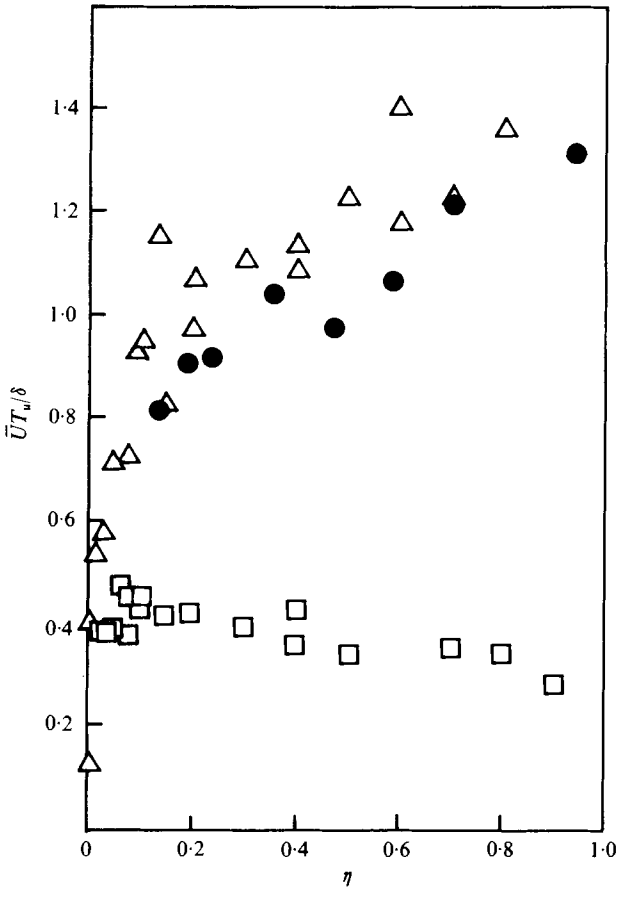

FIGURE 10(*a*). For legend see next page.

Correlograms (curves of R *vs.* T) of u and v fluctuations for flat, convex and concave walls were obtained at several points across the boundary layer. The correlograms over the curved walls, in general, looked similar to those observed in the flat-wall boundary layer. They did not consistently show the presence of any predominant frequencies though some of the correlograms did exhibit some mild fluctuations around the T axis. The correlograms of v fluctuations for the three walls showed some differences in shape. The correlograms for the concave wall showed a long tail and those for the convex wall showed a short tail when compared with the flat-wall correlograms. Many of these features can be observed from the typical correlograms shown in figure 9.

The integral time scales T_u and T_v of the u and v fluctuations were calculated by finding the area under each correlogram up to the point where it first reached zero (as indicated by the arrows on the typical correlograms in figure 9). This procedure was found to be generally satisfactory, since in most cases the correlograms did not have any significant negative lobes. The integral time scale gives a measure of the duration for which the turbulent fluctuations of various frequencies last, on average, before getting destroyed. From figure 9, it can be seen that correlogram 3 for the concave wall has a larger area, indicating a longer average lifetime for the eddies,

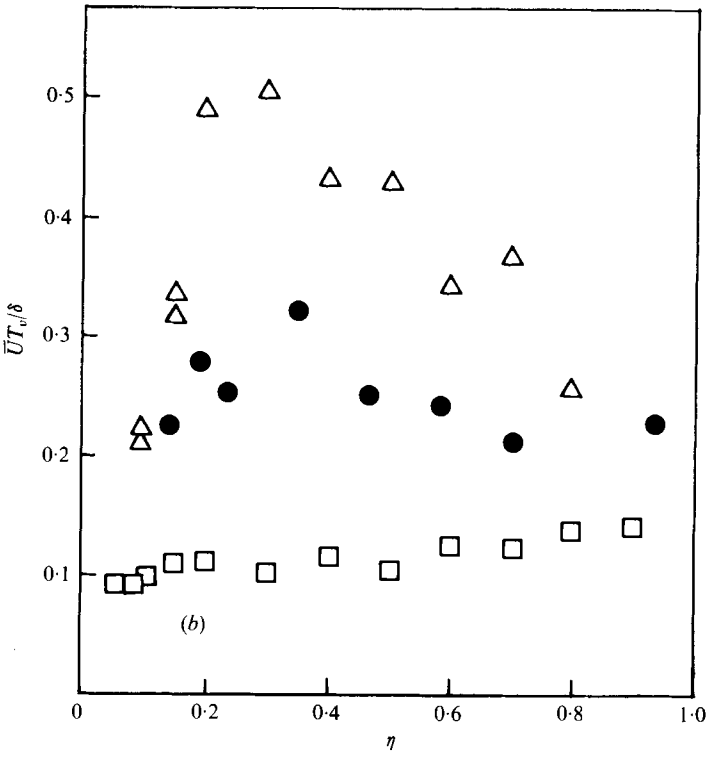

FIGURE 10. The distribution of the non-dimensional length scales of the turbulent velocity fluctuations across the boundary layer. (*a*) u', (*b*) v'. Symbols as in figure 4.

while the correlograms (e.g. 2 and 5) for the convex wall indicate shorter average lifetimes when compared with those (e.g. 1 and 4) over the flat wall. A quantitative description of these features is given in the next paragraph.

Length scales. Using the local mean velocity as the convection velocity, integral length scales of the u and v fluctuations can be obtained from the integral time scales. These have been normalized with respect to the boundary-layer thickness and are plotted in figures 10 (*a*) and (*b*). Large differences can be observed between the convex- and concave-wall length scales for both u and v fluctuations. The *normalized* length scales of the u fluctuation over the concave wall are much larger when compared with those over the convex wall across almost the entire boundary layer. However, the increase over the flat-wall length scale is not very large. On the other hand, over the convex wall there is a large reduction in the length scale of u fluctuations compared with the flat wall. This trend is in conformity with the trend shown by the other flow quantities. The length scales of the v fluctuations show a much larger difference between convex and concave walls compared with the length scales of u fluctuations. Also, the shape of the distribution of v length scales gradually varies from a flatter shape for the convex wall to a peaky shape for the concave wall, with the flat-wall data falling in between. These indicate that the v fluctuations are very sensitive to wall curvature.

The difference in the behaviour of the u and v fluctuations is clearly seen in figure 11, where the ratio T_u/T_v is plotted. Over the convex wall this ratio gradually decreases across the boundary layer from 4 to 2, whereas on the concave wall the ratio first

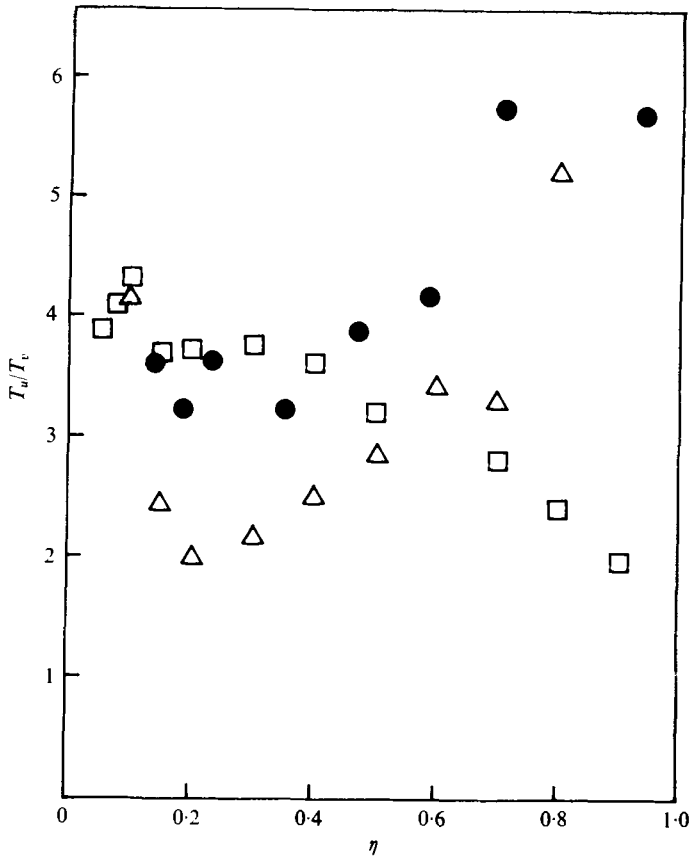

FIGURE 11. The distribution of T_u/T_v across the boundary layer. Symbols as in figure 4.

decreases from 4 to 2 and then increases to a value of 5 in the outer region. This is because, in the case of the concave wall, the length scale of the v fluctuations continuously decreases in the outer layer after it reaches a maximum value around $y/\delta \simeq 0{\cdot}3$. This peculiar behaviour of the length scale in the case of the concave wall is rather unexpected and cannot be explained at this stage. It can, however, be seen that the flat-wall behaviour is approximately intermediate between that for the convex and concave walls. It can also be noted that the values of T_u/T_v shown in figure 11, as well as the length scales themselves (estimated from extrapolation in the case of v fluctuations), are not substantially affected by curvature in the region *close* to the wall.

3.3. *Turbulent spectra*

A few typical normalized auto- and cross-power spectra of the u and v fluctuations are shown in figures 12 (a)–(c) for the three walls. For this purpose, we define the one-dimensional wavenumber k in the usual way, as

$$k = 2\pi f/\overline{U}, \tag{3.3}$$

where f is the frequency. Using the above definition, one can compute the one-

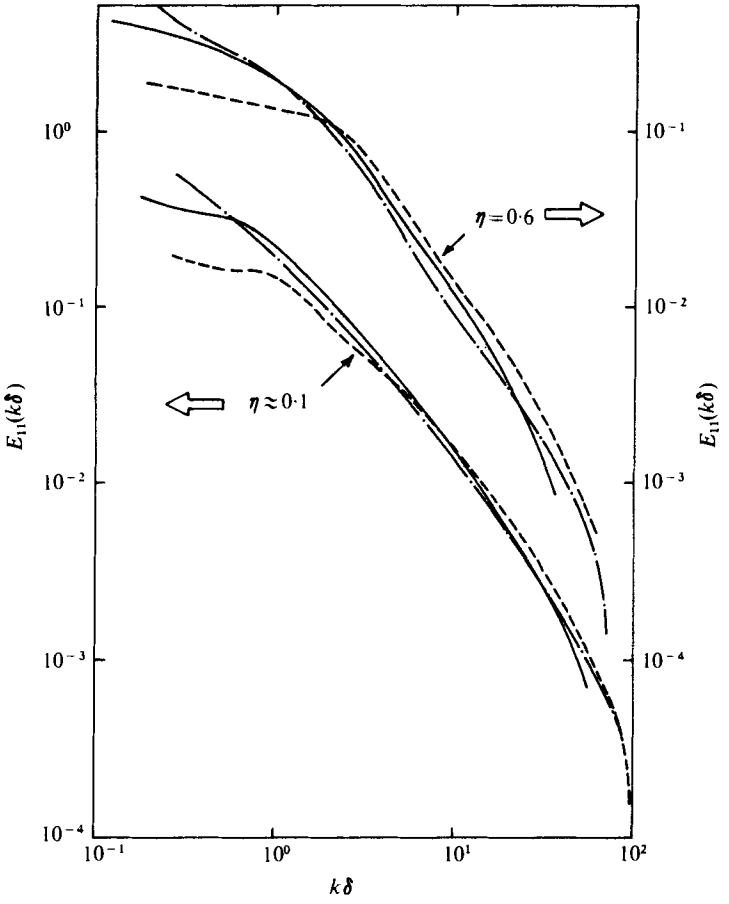

FIGURE 12(*a*). For legend see next page.

dimensional spectral functions in wavenumber space from the measured frequency spectra. The normalized spectral functions $E(k\delta)$ are again defined in the usual way, by the relations

$$\left.\begin{aligned} \int_0^\infty E_{11}(k\delta)\,d(k\delta) &= 1 \quad \text{for the autospectrum of} \quad u'^2, \\ \int_0^\infty E_{22}(k\delta)\,d(k\delta) &= 1 \quad \text{for the autospectrum of} \quad v'^2, \\ \int_0^\infty E_{12}(k\delta)\,d(k\delta) &= 1 \quad \text{for the spectrum of} \quad -\overline{uv}. \end{aligned}\right\} \tag{3.4}$$

Figure 12(*a*) compares the u'^2 spectra for the three walls at two typical points ($y/\delta = 0{\cdot}1$ and $y/\delta = 0{\cdot}6$) in the boundary layer at station 35. From this figure, it can be seen that the spectra for the two curved boundary layers are not significantly different from each other except near the low wavenumber end. The difference at the low wavenumber end leads to the difference in the integral time scales which has already been observed in the plots of the length-scale distributions. It can also be seen from figure 12(*a*) that the spectral distributions of u'^2 in the inner ($\eta = 0{\cdot}1$) and outer ($\eta = 0{\cdot}6$) regions are not generally different from each other.

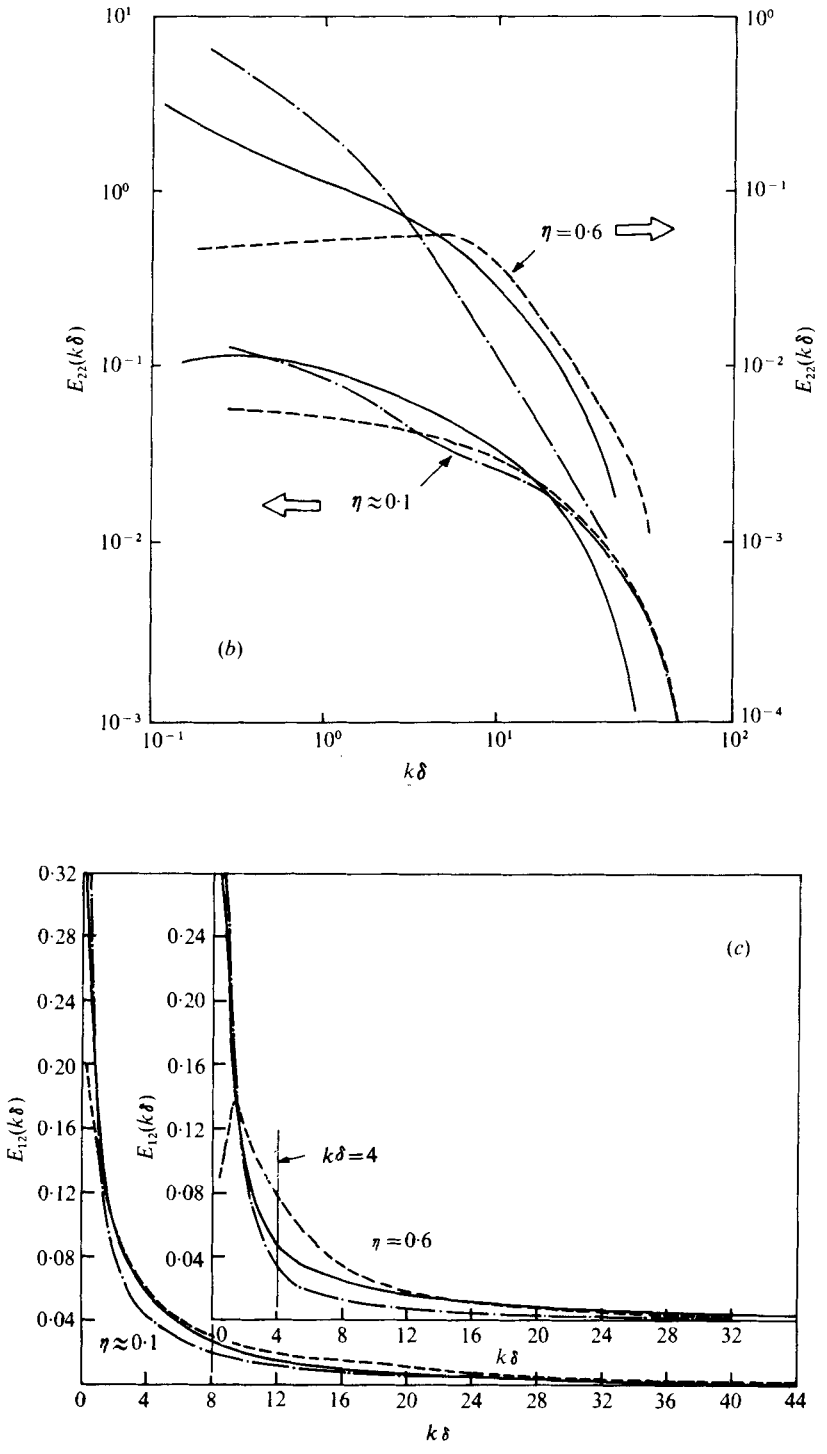

FIGURE 12. Non-dimensional spectra at $\eta \approx 0{\cdot}1$ and $0{\cdot}6$. (*a*) u'^2, (*b*) v'^2, (*c*) $\overline{uv}$. – – – –, convex wall; —·—, concave wall; ——, flat wall. The curved-wall data are for station 35 and the flat-wall data for station 20. The vertical line in (*c*) corresponds to a non-dimensional wavenumber of 4.

In contrast with the above behaviour, the spectral distributions of v'^2 were found to be strongly affected by curvature especially in the outer part of the boundary layer. Two typical distributions at $\eta = 0{\cdot}1$ and $\eta = 0{\cdot}6$ are shown in figure 12(*b*). At $\eta = 0{\cdot}1$ the difference between the spectral distributions for convex and concave walls is very small except at very low wavenumbers. (The authors are unable to explain why, at $\eta = 0{\cdot}1$, the spectra for both curvatures, especially at higher wavenumbers, deviate in the *same* direction from the flat-wall spectra. In fact this behaviour was observed near the outer edge of the boundary layer also ($\eta > 0{\cdot}9$).) However, in the outer layer, the effect of curvature was found to be very strong over the entire wavenumber range as is evident from the data at $\eta = 0{\cdot}6$ in figure 12(*b*). It can be seen that with convex curvature there is a substantial contribution to the spectrum from the high wavenumbers. In fact, even at a non-dimensional wavenumber ($k\delta$) of 20, the contribution is still about 15 % of that at a wavenumber of 0·2. On the other hand, in the case of the concave wall the spectrum drops very steeply, the corresponding contribution being less than 1 %. This means that a large contribution to v'^2 comes from relatively large eddies in the case of the concave wall whereas the contribution is distributed more evenly in the case of the convex wall. Consequently, the development of the flow over the concave wall is influenced by the dynamics of the larger eddies to a greater extent than in the case of flow over the convex wall. The observed strong effect of curvature on the v'^2 spectra and the relatively weak effect on the u'^2 spectra are in general agreement with the observations of Eskinazi & Yeh (1956) in curved-channel flow.

The effect of curvature on the structure of turbulence is again very clearly indicated by the typical spectra of $-\overline{uv}$ presented in figure 12(*c*). These spectra are presented on linear plots as the effects are more clearly brought out this way. Considering the spectra corresponding to $y/\delta = 0{\cdot}6$, it can be seen that in the case of the convex wall about 50 % of the shear stress is produced by eddies smaller than $\frac{1}{4}$ of the boundary-layer thickness (the $k\delta$ corresponding to this is shown by a line in the figure), whereas on the concave wall the contribution to the $\overline{uv}$ from eddies smaller than $\frac{1}{4}$ of the boundary-layer thickness is only about 25 %. Thus it is seen that the increased shear stress observed on the concave wall essentially comes from the relatively larger eddies. These larger eddies are suppressed over the convex wall with a consequent reduction in the shear stress. The flat wall is seen to have a trend intermediate between convex and concave walls. Again, the contrast between the results for the two walls is seen to be less strong in the inner region ($y/\delta = 0{\cdot}1$) than in the outer region ($y/\delta = 0{\cdot}6$).

3.4. *Amplitude probability distributions*

The amplitude probability density distributions of the u and v signals are shown in figures 13(*a*)–(*c*) for the flat as well as curved walls at a few typical points across the boundary layer. For comparison, the Gaussian distribution is also shown. The distributions have been normalized with respect to the maximum probability density and half the width of the distribution curve at 10 % of the maximum probability density. In figures 13(*a*)–(*c*), P^* and A^* are the normalized probability density and amplitude so obtained. The maximum probability density did not occur at zero amplitude, though the amplitude at maximum probability density was quite small in each case. (This can be seen from figures 13(*b*) and (*c*), where the origins for the distribution curves are shown for two typical cases.) Hence for easy comparison the distribution curves

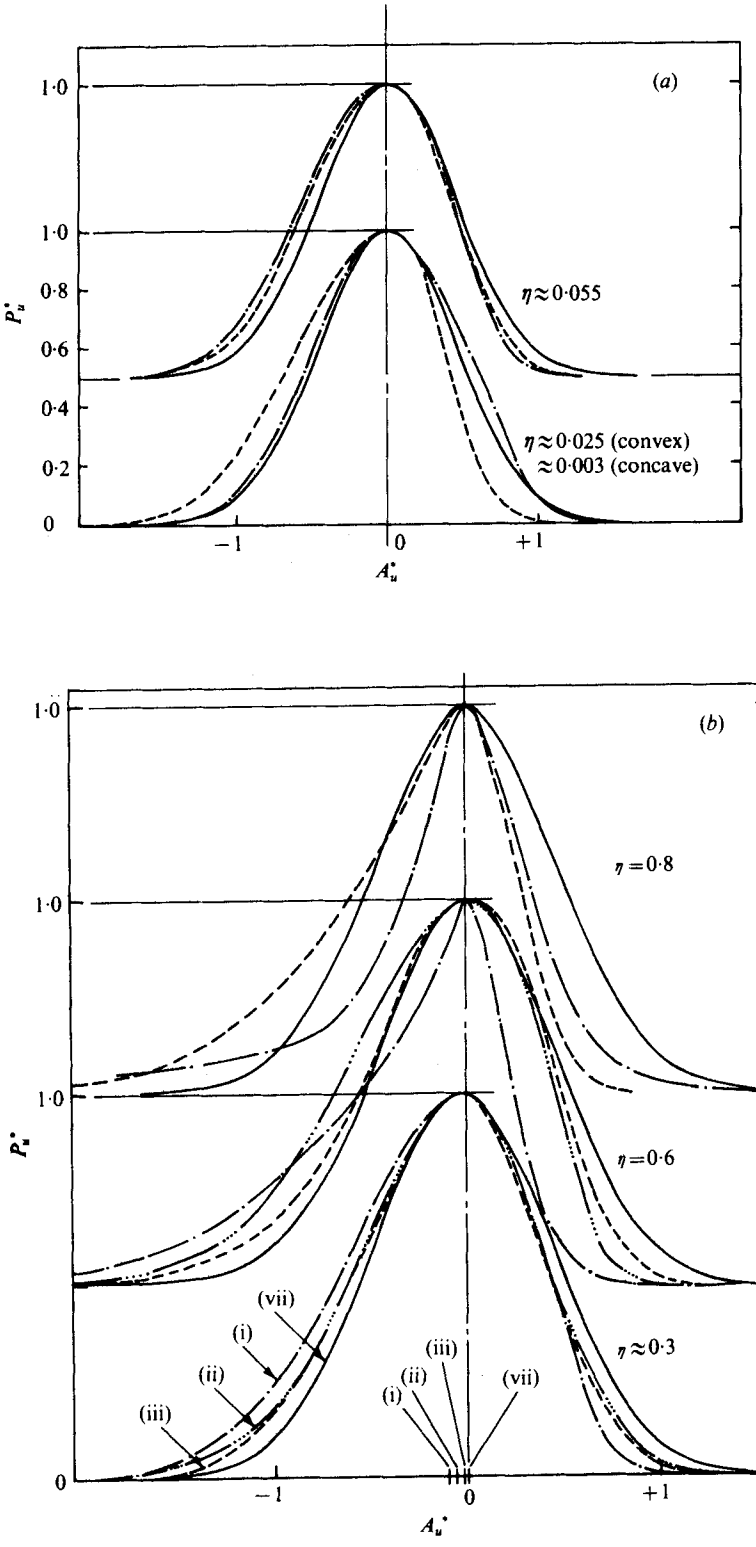

FIGURES 13 (*a*, *b*). For legend see facing page.

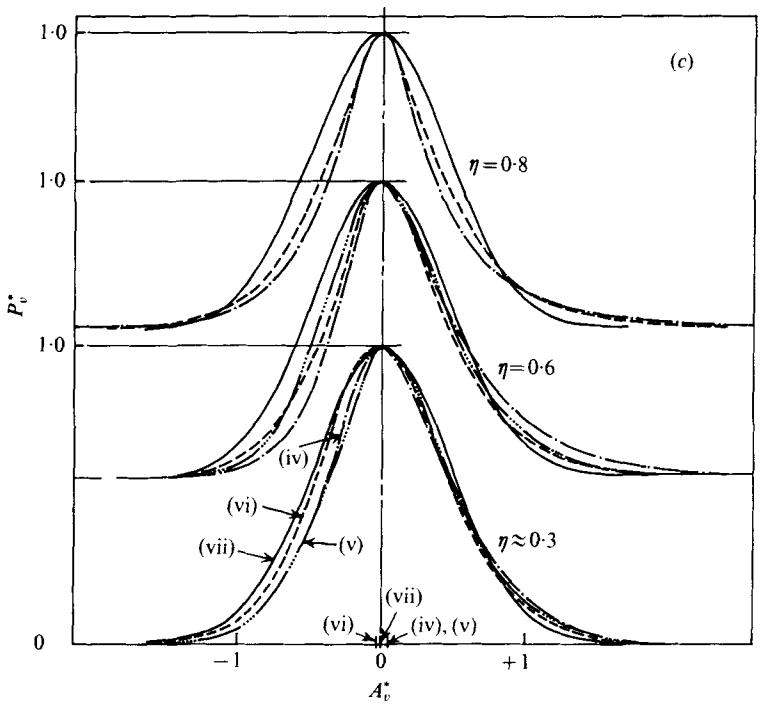

FIGURE 13. Amplitude probability density distributions of the turbulent velocity fluctuations: (*a*) u' in the inner region ($\eta \leqslant 0{\cdot}1$), (*b*) u' in the outer region $\eta > 0{\cdot}1$, (*c*) v'. ----, convex wall; —·—, concave wall; —·····—, flat wall; ——, Gaussian distribution. The distributions are shown with their apices rather than their origins coinciding. The origins are shown in some typical cases, viz. for curves (i)–(vii).

have been placed in such a way that their apices rather than their origins coincide with one another. It can be seen from the figures that the curves for the u fluctuations are generally more skewed than the curves for the v fluctuations. Also, the direction of skew is opposite for the two fluctuations. That is, the curve for the u fluctuations has a negative tail whereas the curve for the v fluctuations has a positive tail. It is also seen that near the wall the curves for u fluctuations are nearly symmetrical and become more and more skewed as the distance from the wall is increased. Comparison of the curves for the two curvatures shows that the effect of curvature is quite strong in the case of the u fluctuations. It is observed that concave curvature increases the skewness while convex curvature tends to reduce it. In fact, in the case of the concave wall the skewness can be detected from $y/\delta = 0{\cdot}3$. The curve for the convex wall at the same value of y/δ indicates a more nearly symmetrical distribution. In a few typical cases, the distributions (at approximately the same values of y/δ) corresponding to the flat wall at station 20 are also provided for comparison. It can be seen that generally the deviations from the flat-wall distribution are on opposite sides for the two curvatures.

The effect of curvature in the case of the v fluctuations is apparently quantitatively small everywhere in the boundary layer. It is, however, important to point out that the curves in figure 13(*c*) show the probability distributions of the fluctuations from the mean value and do not give any information on the shift in the mean value itself.

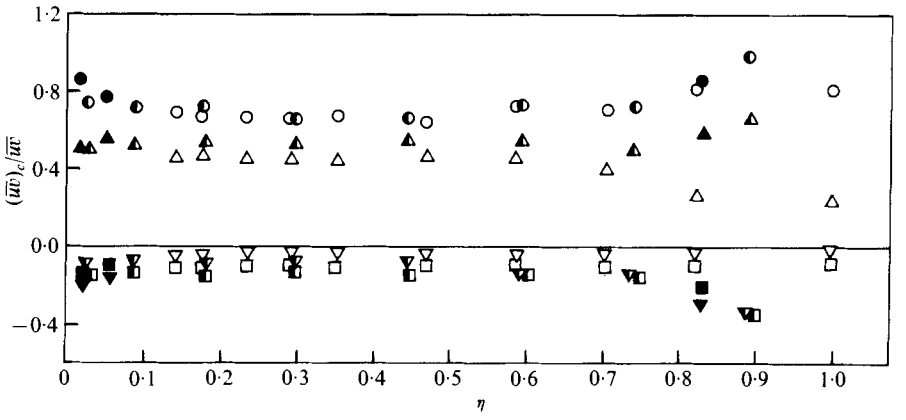

FIGURE 14. Conditional correlations in flat-wall boundary layers.

$\overline{u_+v_+}$	$\overline{u_-v_-}$	$\overline{u_+v_-}$	$\overline{u_-v_+}$	
■	▼	▲	●	Lu & Willmarth (1973)
◧	▽	◭	◐	Rajagopalan (1974)
□	▽	△	○	Present experiments (station 20).

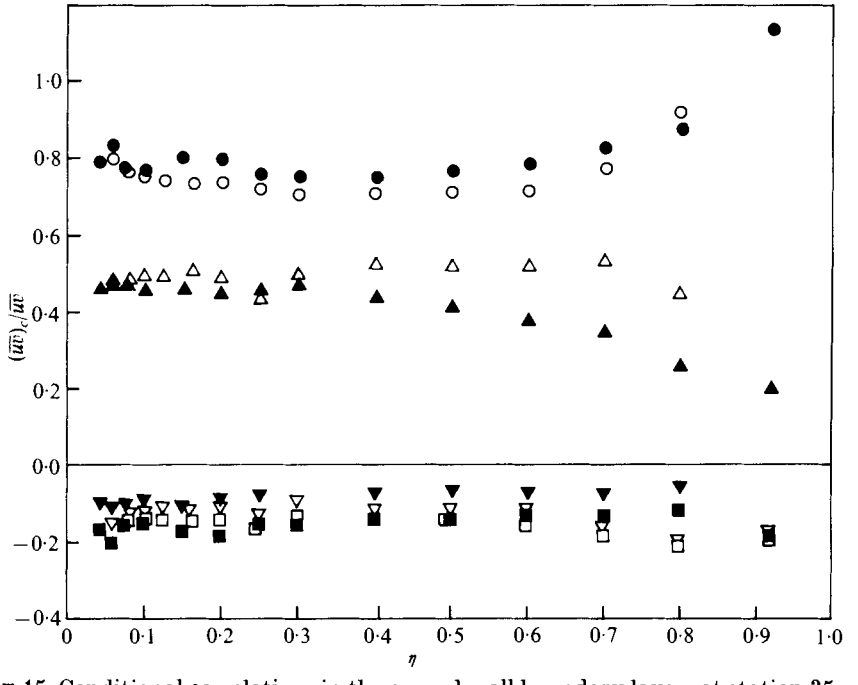

FIGURE 15. Conditional correlations in the curved-wall boundary layers at station 35.

$\overline{u_+v_+}$	$\overline{u_-v_-}$	$\overline{u_+v_-}$	$\overline{u_-v_+}$	
□	▽	△	○	Convex wall
■	▼	▲	●	Concave wall

Component	Contribution as a percentage of $(-\overline{uv})$	
	Concave wall	Convex wall
$\overline{u_-v_+}$	+79	+72
$\overline{u_+v_-}$	+39	+53
$\overline{u_+v_+}$	−11·5	−15
$\overline{u_-v_-}$	−6·5	−10

TABLE 1

This shift can be quite significant over the curved walls as will be seen from the discussion in § 3.6.

3.5. *Conditional correlations*

As mentioned earlier, the effect of curvature on the turbulence structure has been explained from stability considerations in the past. For a better and more detailed understanding of this effect, a study of the various turbulent motions and their contribution to the Reynolds stresses will be very helpful. Such studies in the past have been very useful in understanding the mechanism of turbulent production and transport in flat-wall boundary layers (e.g. Wallace *et al.* 1972; Willmarth & Lu 1972; Lu & Willmarth 1973; Badri Narayanan, Rajagopalan & Narasimha 1974). It is for this reason that conditional correlations were measured in the present case. These measurements are used to study the effect of curvature on the different turbulent motions.

The distributions across the boundary layer of the four conditional correlations $(\overline{uv})_c$ representing the contribution to the Reynolds shear stress are shown in figures 14 and 15. Of these, figure 14 shows the data for the flat-wall boundary layer at station 20. This figure also shows similar flat-wall data from the work of Lu & Willmarth (1973) and Rajagopalan (1974). The agreement between the present and earlier results seems to be generally satisfactory and thus establishes confidence in the measurement technique used.

The distributions of these components in the case of the curved walls are shown in figure 15. It can be observed that, over the concave wall, especially in the outer layer, the shear stress $-\rho\overline{uv}$ is increased owing to an increase in the negative contribution from the $\overline{u_-v_+}$ component and the suppression of the positive contributions from the $\overline{u_+v_+}$ and $\overline{u_-v_-}$ components. It is interesting to note that the magnitude of the contribution from $\overline{u_+v_-}$ is, in fact, *reduced* in the case of the concave wall. At a typical outer location, say $y/\delta = 0{\cdot}6$, the relative contributions measured were as given in table 1. For ease of reference, we can denote the top two components in the above table as 'dominant' components and the bottom two as 'occasional' components. It can be seen from the above table that, in the case of the concave wall, both the components associated with positive fluctuations of u are suppressed while the dominant component associated with negative fluctuations of u is enhanced. This means that the negative fluctuations in u would be relatively more vigorous in the boundary layer over the concave wall. This conclusion is also substantiated by the distributions of the ratio $\overline{u_-^2}/\overline{u_+^2}$, shown in figure 16. It is seen that the ratio is larger for the concave wall than for the convex wall. Since u and v are negatively correlated, one would expect to see qualitatively similar behaviour of the ratio $\overline{v_+^2}/\overline{v_-^2}$. This ratio, plotted in figure 16,

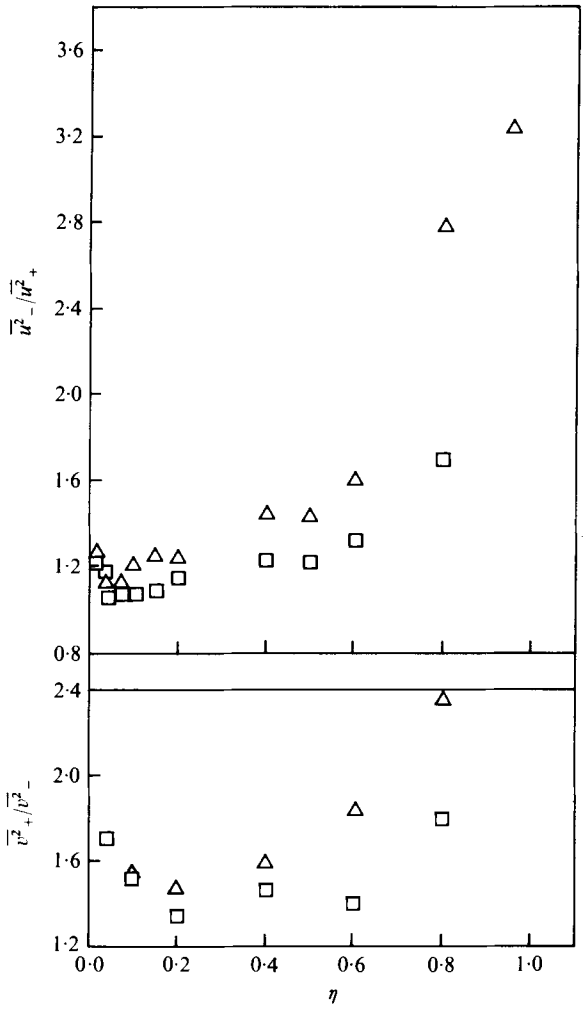

FIGURE 16. The distributions of the ratios $\overline{u^2_-}/\overline{u^2_+}$ and $\overline{v^2_+}/\overline{v^2_-}$ across the curved boundary layers. □, convex wall; △, concave wall.

exhibits the expected trend. These results from the conditional correlation measurements are also consistent with those obtained from the probability distributions shown in figures 13(*a*)–(*c*).

3.6. *Turbulent transport within the boundary layer*

The detailed measurements of various quantities within the boundary layer reported so far have provided sufficient information to enable one to form some conclusions about the influence of curvature on the mechanism of turbulent transport in the boundary layer. The distributions of the diffusion term for convex and concave walls shown in figures 7 and 8 have clearly indicated that curvature has a significant effect on the transport of turbulent kinetic energy and pressure energy. The modification of the transport of these quantities over the curved walls can be attributed to the

behaviour of the v fluctuations in the boundary layer. For example, the radial pressure gradient inhibits the v_+ fluctuations on the convex wall and aids them on the concave wall. As a result the outward flux $\overline{v(\frac{1}{2}q^2+p/\rho)}$ is reduced over the convex wall and enhanced over the concave wall. The generally steeper gradient of kinetic energy over the convex wall and a smaller gradient over the concave wall tend to oppose the above effect but apparently are not strong enough to reverse the trend.

The transport of momentum across the boundary layer (as represented by the Reynolds stress) is affected by curvature likewise as has been seen from figure 15. However, the nature of the influence of curvature on this transport is more complicated than in the case of the turbulent energy transport. This is because the diffusion flux of momentum $-\rho\overline{uv}$ depends on the behaviour of both u and v fluctuations. In addition to the direct effect of the radial pressure gradient, which favours the v fluctuations of a particular sign, the changes in the centrifugal force brought about by fluctuations in u tend to influence the v fluctuations indirectly. The momentum transport is thus determined by the interaction of the effects of the radial pressure gradient, the centrifugal force and the gradient of mean velocity. This interaction produces different effects on the four different component conditional correlations shown in figure 15. For example, let us consider the conditional correlation $\overline{u_-v_+}$. If a turbulent lump located at a point decelerates momentarily, the centrifugal force on the lump decreases and therefore it drifts to an orbit of lesser radius. In the case of the boundary layer over the concave wall this motion would contribute to an increase in the product $\overline{u_-v_+}$. This contribution is additional to the already enhanced contribution due to the favoured v_+ motions on the concave wall induced by the radial pressure gradient even when the lump is moving with constant longitudinal velocity. An opposite effect can be expected over the convex wall. Second, the velocity gradient over a large part of the concave-wall boundary layer is smaller than that over the convex wall. From elementary mixing-length arguments it is easy to see that this should reduce momentum transport (i.e. reduce the magnitude of the negative product $\overline{u_-v_+}$) over the concave wall and increase it over the convex wall. From figure 15, it can be seen that the combined influence of the radial pressure gradient and the centrifugal force is not fully countered by the effect of relatively smaller velocity gradients over the concave wall, thus resulting in a slightly larger value of the $\overline{u_-v_+}$ component in the case of the concave wall compared with the convex wall.

Considering now the other dominant component, namely $\overline{u_+v_-}$, the effect of the radial pressure gradient is to suppress the v_- motions over the concave wall and enhance them over the convex wall. On the other hand any local instantaneous acceleration of a fluid lump will aid the v_- motions owing to the effect of the centrifugal force in the case of the convex wall. Finally, the smaller mean velocity gradient in the case of the concave wall tends to suppress the transport of momentum in general, thus leading to a reduction in the $\overline{u_+v_-}$ component. In contrast to this, in the case of the convex wall the larger velocity gradient leads to an increased $\overline{u_+v_-}$ component. The net result of all these effects can be observed from figure 15 as (surprisingly) a net decrease of $\overline{u_+v_-}$ in the case of the concave wall compared with the convex wall.

In a similar way, the implications of the interaction on the components $\overline{u_+v_+}$ and $\overline{u_-v_-}$ can also be analysed.

It is thus clear that curvature can affect the transport of momentum and turbulent

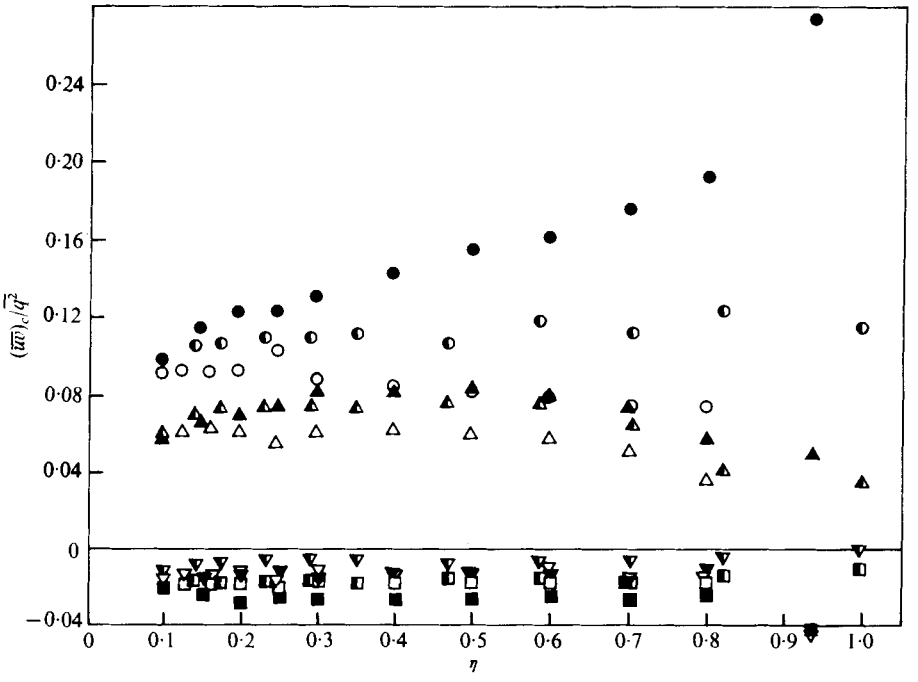

FIGURE 17. Componentwise contributions to $-\overline{uv}/\overline{q^2}$.

kinetic energy to different extents. Also results presented so far have indicated that very close to the wall the nature of the flow (e.g. the law of the wall, the non-dimensional distribution of $-\overline{uv}/\overline{q^2}$ etc.) is not significantly affected by mild curvature. The effect on the turbulence structure further away from the wall can perhaps be attributed to the curvature-sensitive diffusion process. The distribution of $-\overline{uv}/\overline{q^2}$ shown in figure 1(*d*) can be explained as presumably due to the different effects of curvature on the transports of momentum and turbulent kinetic energy. Apparently, the net effect of curvature is to cause greater changes in the $\overline{uv}$ distribution than in the $\overline{q^2}$ distribution, resulting in a change in the turbulence structure (of which $-\overline{uv}/\overline{q^2}$ is a very good indication) at large distances from the wall. The component-wise contributions to $-\overline{uv}/\overline{q^2}$ are shown in figure 17, from which it is seen that particularly the dominant components (the negative components which contribute a large amount to the Reynolds stress) are increased in magnitude by concave curvature and reduced by convex curvature compared with their values for the flat wall. The changes are however such as to cause a net increase of $-\overline{uv}/\overline{q^2}$ over the concave wall and a net decrease over the convex wall.

The foregoing discussion suggests that the structure of turbulence in the boundary layer over the curved walls is to a large extent affected by the relative diffusion of momentum and turbulent kinetic energy. These diffusions are influenced to a considerable extent by the behaviour of v fluctuations. These fluctuations are affected by

curvature, either directly through the radial pressure gradient or indirectly through the variations in the centrifugal force arising from u fluctuations. The spectral measurements support the conclusion that curvature primarily affects the v fluctuations. Further, the distributions of the integral time scales referred to earlier showed a more systematic effect of curvature on the v fluctuations. Also, it can be shown from the equation for the turbulent kinetic energy of the v fluctuations that curvature results in direct production of v fluctuations in addition to their production during the transfer of momentum from the u motions (see, for example, Eskinazi & Yeh 1956). In view of all this, it appears that turbulent transport models for curved flows are likely to be successful if they are so formulated as to account for the effect of streamline curvature on some characteristic feature of the v fluctuations such as a length scale, velocity scale, etc. No attempt will, however, be made in the present paper to develop a turbulence model for curved flows. A study in this direction is being reported separately.

4. Conclusions

The investigation has led to the following conclusions.

(i) The rate of turbulent energy production is significantly affected by convex curvature. Most of the turbulent production in this case is confined to a region very close to the wall and this region is even smaller than for a flat-wall boundary layer. Mild concave curvature, however, does not seem to affect the production of turbulent energy significantly.

(ii) Even mild wall curvature affects significantly the process of turbulent diffusion in the boundary layer. Convex curvature suppresses both the amount of outward diffusion of turbulent kinetic energy from the wall region and the extent of the region which receives turbulent energy from the wall region. Concave curvature has exactly the opposite effect. This results in a reduction in the extent of the log region over the convex wall and its increase over the concave wall as observed from the mean velocity profiles in figure 1 (*a*).

(iii) The integral time scales T_u and T_v of the turbulent fluctuations are very strongly affected by even mild curvature. The effect is especially spectacular with convex curvature. Further, both autocorrelation and spectral measurements indicate that curvature has a larger effect on the v fluctuations than on the u fluctuations.

(iv) Cross-spectral measurements indicate that, over the convex wall, about 50 % of the contribution to the Reynolds shear stress comes from eddies smaller than $\frac{1}{4}$ of the boundary-layer thickness, whereas, over the concave wall, eddies of this range contribute only to 25 % of the shear stress. The combination of reduced shear stress and shift of the spectrum to the high wavenumber end over the convex wall (and a corresponding opposite combination over the concave wall) suggests that it is the structure of the larger eddies that is sensitive to wall curvature.

(v) Diffusion of both momentum and turbulent kinetic energy is inhibited by convex curvature and enhanced by concave curvature. However, the nature of the effect of curvature on the diffusion process is different for the two properties. This difference is presumably the reason for the observed decrease in the ratio $|(\overline{uv}/\overline{q^2})|$ over the convex wall and its increase over the concave wall compared with the value for the flat-wall boundary layers.

(vi) While the detailed effect of curvature on the various turbulent motions is complex, it can generally be said that v_+ motions are favoured and v_- motions inhibited over the concave wall, the opposite being true for the convex wall. The enhanced v_+ motions over the concave wall cause the amplitude probability distribution of the u fluctuations to be perceptibly skewed towards negative amplitudes over the outer 70 % of the boundary layer.

The authors wish to thank the authorities and staff of the Instrumentation Division of the Aeronautical Development Establishment at Bangalore for making available their tape recorder and Fourier analyser and extending their help in processing the data.

REFERENCES

BADRI NARAYANAN, M. A., RAJAGOPALAN, S. & NARASIMHA, R. 1974 Some experimental investigations of the fine scale structure of turbulence. *Dept. of Aero. Engng, Indian Inst. Sci., Bangalore, Rep.* no. 74 FM 15.

BRADSHAW, P. 1967 The turbulence structure of equilibrium boundary layers. *J. Fluid Mech.* **29**, 625.

BRADSHAW, P. 1969 The analogy between streamline curvature and buoyancy in turbulent shear flow. *J. Fluid Mech.* **36**, 177.

BRADSHAW, P. 1973 Effects of streamline curvature on turbulent flow. *AGARDograph* no. 169.

CASTRO, I. P. & BRADSHAW, P. 1976 The turbulence structure of a highly curved mixing layer. *J. Fluid Mech.* **73**, 267.

ELLIS, L. B. & JOUBERT, P. N. 1974 Turbulent shear flow in a curved duct. *J. Fluid Mech.* **62**, 65.

ESKINAZI, S. & YEH, H. 1956 An investigation on fully developed turbulent flows in a curved channel. *J. Aero. Sci.* **23**, 23.

HINZE, J. O. 1959 *Turbulence.* McGraw-Hill.

IRWIN, H. P. A. H. & SMITH, P. A. 1975 Prediction of the effect of streamline curvature on turbulence. *Phys. Fluids* **18**, 624.

JOHNSTON, J. P. & EIDE, S. A. 1976 Turbulent boundary layers on centrifugal compressor blades: prediction of the effects of surface curvature and rotation. *A.S.M.E. 21st Ann. Int. Gas Turbines Conf., New Orleans*, paper 76-FE-10.

KLEBANOFF, P. S. 1954 Characteristics of turbulence in a boundary layer with zero pressure gradient. *N.A.C.A. Tech. Note* no. 3178.

LAUFER, J. 1954 The structure of turbulence in a fully developed pipe flow. *N.A.C.A. Tech. Note* no. 2954.

LU, S. S. & WILLMARTH, W. W. 1973 Measurements of the structure of Reynolds stress in a turbulent boundary layer. *J. Fluid Mech.* **60**, 481.

MAGRAB, E. B. & BLOMQUIST, D. S. 1971 *The Measurement of Time-Varying Phenomena.* Interscience.

MERONEY, R. N. & BRADSHAW, P. 1975 Turbulent boundary layer growth over a longitudinally curved surface. *A.I.A.A. J.* **13**, 1448.

PAPAILIOU, K. D., NURZIA, F. & SATTA, A. 1970 The inclusion of surface curvature effects in the calculation of the turbulent boundary layer with integral methods. *Von Kármán Inst. Fluid Dyn. Internal Note* no. 37.

PATEL, V. C. 1968 The effects of curvature on the turbulent boundary layer. *Aero. Res. Counc. R. & M.* no. 3599.

RAJAGOPALAN, S. 1974 Some experimental investigations of the fine scale structure of turbulence. Ph.D. thesis, Dept. Aeronautical Engineering, Indian Institute of Science, Bangalore.

RAMAPRIAN, B. R. & SHIVAPRASAD, B. G. 1977 Mean flow measurements in turbulent boundary layers along mildly curved surfaces. *A.I.A.A. J.* **15**, 189.

RASTOGI, A. K. & WHITELAW, J. H. 1971 Procedure for predicting the influence of longitudinal curvature of boundary-layer flows. *A.S.M.E. Winter Ann. Meeting, Washington, D.C.*, paper 71-WA/FE-37.

SCHMIDBAUER, H. 1936 Behaviour of turbulent boundary layers on curved convex wall. *N.A.C.A. Tech. Memo.* no. 791.

SHIVAPRASAD, B. G. 1976 An experimental study of the effect of mild longitudinal curvature on the turbulent boundary layer. Ph.D. thesis, Dept. Aeronautical Engineering, Indian Institute of Science, Bangalore.

SHIVAPRASAD, B. G. & RAMAPRIAN, B. R. 1977 Turbulence measurements in boundary layers along mildly curved surfaces. *A.S.M.E. Winter Ann. Meeting, Atlanta*, paper 77-WA/FE-6 (to appear in *J. Fluids Engng*).

So, R. M. C. 1975 A turbulence velocity scale for curved shear flows. *J. Fluid Mech.* **70**, 37.

So, R. M. C. & MELLOR, G. L. 1972 An experimental investigation of turbulent boundary layers along curved surfaces. *N.A.S.A. Contractor Rep.* no. 1940.

So, R. M. C. & MELLOR, G. L. 1973 Experiment on convex curvature effects in turbulent boundary layers. *J. Fluid Mech.* **60**, 43.

So, R. M. C. & MELLOR, G. L. 1975 Experiment on turbulent boundary layers on a concave wall. *Aero. Quart.* **26**, 25.

TANI, I. 1962 Production of longitudinal vortices in the boundary layer along a concave wall. *J. Geophys. Res.* **67**, 3075.

WALLACE, J. M., ECKELMANN, H. & BRODKEY, R. S. 1972 The wall region in turbulent shear flow. *J. Fluid Mech.* **54**, 39.

WATTENDORF, F. L. 1935 A study of the effect of curvature on fully developed turbulent flow. *Proc. Roy. Soc.* A **148**, 565.

WILLMARTH, W. W. & LU, S. S. 1972 Structure of Reynolds stress near the wall. *J. Fluid Mech.* **55**, 65.